Molecular Biology of the Cell
Vol. 21, 3182–3192, September 15, 2010

Cortical Mechanics and Meiosis II Completion in Mammalian Oocytes Are Mediated by Myosin-II and Ezrin-Radixin-Moesin (ERM) Proteins

Stephanie M. Larson,*† Hyo J. Lee,*† Pei-hsuan Hung,* Lauren M. Matthews,* Douglas N. Robinson,‡§ and Janice P. Evans*

*Department of Biochemistry and Molecular Biology, Bloomberg School of Public Health, and ‡Department of Cell Biology, and §Department of Pharmacology and Molecular Sciences, School of Medicine, Johns Hopkins University, Baltimore, MD 21205

Submitted January 28, 2010; Revised July 1, 2010; Accepted July 12, 2010
Monitoring Editor: Yu-Li Wang

Cell division is inherently mechanical, with cell mechanics being a critical determinant governing the cell shape changes that accompany progression through the cell cycle. The mechanical properties of symmetrically dividing mitotic cells have been well characterized, whereas the contribution of cellular mechanics to the strikingly asymmetric divisions of female meiosis is very poorly understood. Progression of the mammalian oocyte through meiosis involves remodeling of the cortex and proper orientation of the meiotic spindle, and thus we hypothesized that cortical tension and stiffness would change through meiotic maturation and fertilization to facilitate and/or direct cellular remodeling. This work shows that tension in mouse oocytes drops about sixfold during meiotic maturation from prophase I to metaphase II and then increases ~1.6-fold upon fertilization. The metaphase II egg is polarized, with tension differing ~2.5-fold between the cortex over the meiotic spindle and the opposite cortex, suggesting that meiotic maturation is accompanied by assembly of a cortical domain with stiffer mechanics as part of the process to achieve asymmetric cytokinesis. We further demonstrate that actin, myosin-II, and the ERM (Ezrin/Radixin/Moesin) family of proteins are enriched in complementary cortical domains and mediate cellular mechanics in mammalian eggs. Manipulation of actin, myosin-II, and ERM function alters tension levels and also is associated with dramatic spindle abnormalities with completion of meiosis II after fertilization. Thus, myosin-II and ERM proteins modulate mechanical properties in oocytes, contributing to cell polarity and to completion of meiosis.

INTRODUCTION

The meiotic divisions of the oocyte have significant impact on reproductive and developmental success, even though the first of these divisions occurs before a mammalian embryo is even created and the second occurs shortly after sperm has penetrated. In these two meiotic cell divisions, chromosomes must be segregated evenly between the daughter cells, as most aneuploidies are lethal or cause congenital birth defects (Hassold and Hunt, 2001). The other cellular contents must be distributed very asymmetrically, so that the egg cytoplasm retains the materials that were stockpiled during oogenesis to support early embryo development. Thus, the meiotic divisions create a large egg and small polar bodies. Female meiosis also has unique temporal challenges, with meiosis occurring in a staggered manner, characterized by an arrest at prophase I (which can last for days and up to years, depending on the species), then another arrest at metaphase II (MII) in most mammals (which can last for hours), and finally creation of the haploid maternal genome component occurring only after fertilization occurs.

Progression through meiosis is accompanied by changes in cortical architecture. These changes in the egg cortex are important for several reasons. The egg cortex has long been appreciated as having a key role in embryogenesis in localizing maternal determinants and in axis determination (reviewed in Sardet *et al.*, 2002). Recent work also shows that the egg cortex functions in earlier stages of embryo development, involved in responses to sperm and the egg-to-embryo transition (Esposito *et al.*, 2007; FitzHarris *et al.*, 2007; Maruyama *et al.*, 2007; Stitzel *et al.*, 2007; Li *et al.*, 2008b; Cheng *et al.*, 2009; Parry *et al.*, 2009). Additionally, remodeling of the cortex accompanies progression of the prophase I, germinal vesicle-intact (GVI) oocyte to the MII stage, and this cortical remodeling is part of the creation of cellular asymmetry (Brunet and Maro, 2005). The MII-arrested mouse egg has two distinct regions of the egg plasma membrane and cortex: the amicrovillar domain, which sequesters the meiotic spindle and is enriched in actin filaments, and the microvillar domain to which sperm bind and fuse. Formin-2, myosin-II, and the small GTPases Rac, Cdc42, and

This article was published online ahead of print in *MBoC in Press* (http://www.molbiolcell.org/cgi/doi/10.1091/mbc.E10–01–0066) on July 21, 2010.

†These authors contributed equally to this work.

Address correspondence to: Douglas N. Robinson (dnr@jhmi.edu) or Janice P. Evans (jpevans@jhsph.edu).

Ran have been implicated through a variety of studies (gene knockout studies, RNAi, pharmacological perturbation, antibody injection) in the movement of the spindle to the cortex during metaphase I (MI) and/or the associated remodeling of cortical actin (Simerly *et al.,* 1998; Leader *et al.,* 2002; Na and Zernicka-Goetz, 2006; Deng *et al.,* 2007; Halet and Carroll, 2007; Li *et al.,* 2008a; Schuh and Ellenberg, 2008). However, the effects of cortical dynamics on meiosis, particularly the second meiotic division, are still not fully understood.

Given the morphological changes that occur during oocyte maturation and fertilization, we hypothesized that the mechanical characteristics of the oocyte would vary with these developmental transitions to facilitate and/or direct cellular remodeling. The mechanical properties of a cell are a critical determinant governing cell shape changes, such as those occurring during mitotic cytokinesis or cellular morphogenesis, and affecting cellular characteristics such as deformability (Zhang and Robinson, 2005; Kunda *et al.,* 2008; Reichl *et al.,* 2008). Here, we use micropipette aspiration (MPA) to measure the mechanical properties of mouse oocytes. Because cells are neither purely elastic solids nor fluids with constant surface tensions, the response to applied pressure may reflect multiple mechanical properties. Therefore, we measure an effective tension (T_{eff}), which is an energy cost for adding a unit of surface area and reflects both the tension and the stretch or expansivity modulus (Derganc *et al.,* 2000; Reichl *et al.,* 2008). This quantitative metric reflects the biochemical and structural features of the cortex, which are mediated by force generation from actin assembly and myosin-II motor activity, along with the structural organization of actin polymers and linkages between the polymers and the membrane. Actin-cross–linking proteins and filament-membrane–tethering proteins can also contribute to this structural organization and to mechanical properties of the cell by mediating the associations between actin polymers.

Cellular mechanical properties have been studied in echinoderm and amphibian eggs and early embryos, providing insights into how these mechanical properties were affected by temperature, by culture conditions, and most importantly, by fertilization and progression through embryonic mitosis (Cole, 1932; Cole and Michaelis, 1932; Harvey and Fankhauser, 1933; Mitchison and Swann, 1954, 1955; Mitchison and Swann, 1954, 1955; Selman and Waddington, 1955; Wolpert, 1966; Rappaport, 1967; Sawai and Yoneda, 1974; Hiramoto, 1976), although there is only limited information about mechanical transitions in different cellular regions of eggs or during meiosis (Sawai and Yoneda, 1974; Hiramoto, 1976; Nakamura and Hiramoto, 1978). This article presents the first characterization of quantifiable mechanics in mammalian eggs, showing that there are dramatic dynamics in cellular mechanics in mouse oocytes with progression through meiosis as well as a mechanical polarity established at MII arrest. We also demonstrate the contributions of actin, nonmuscle myosin-II, and Ezrin/Radixin/Moesin (ERM) proteins to cellular mechanics in oocytes. The members of the ERM family mediate cytoskeletal-membrane interactions (Bretscher *et al.,* 2002; Fehon *et al.,* 2010). Flies deficient in *Moesin* (the only *Drosophila* ERM protein) have abnormalities in oocyte polarity, actin organization, and localization of certain maternal determinants such as Oskar and Staufen (Jankovics *et al.,* 2002; Polesello *et al.,* 2002). RNAi studies of cultured *Drosophila* cells and of *Dictyostelium* cells show that ERM proteins contribute to cortical mechanics (moesin in *Drosophila*; Carreno *et al.,* 2008; Kunda *et al.,* 2008; and enlazin, the closest ERM relative in *Dictyostelium*; Octtaviani *et al.,* 2006). Radixin is among the most abundant mRNAs detected in mouse oocyte transcriptomes (e.g., Evsikov *et al.,* 2006, and Unigene library IDs 18552, 10029, and 14142), and mouse eggs have been reported to express ezrin protein (Louvet *et al.,* 1996). Here, we find that mouse eggs also express radixin and moesin proteins, and activated forms of these proteins enrich in the microvillar domain, complementary to actin and myosin II, which are enriched in the amicrovillar domain. The disruption of ERM function by expression of a dominant-negative form of radixin, perturbation of actin, or inhibition of myosin-II reduced effective tension in MII eggs, as well as produced dramatic spindle abnormalities during exit from MII after fertilization.

MATERIALS AND METHODS

GVI Prophase I Oocytes, Metaphase II Eggs, Sperm, and Zygotes

Collection of oocytes from CF-1 mice (Harlan, Indianapolis, IN) and zona pellucida (ZP) removal were performed as described (Evans *et al.,* 2000). Whitten's medium (Whitten, 1971) was supplemented with 2.5 μM milrinone (Sigma-Aldrich, St. Louis, MO) or 100 mM dbcAMP (Sigma-Aldrich) to maintain prophase I arrest (Cho *et al.,* 1974; Tsafriri *et al.,* 1996). Oocytes were matured in vitro in medium lacking milrinone/dbcAMP. Germinal vesicle breakdown (GVBD) stage and MI samples were prepared at 4 h and 9 h after milrinone/dbcAMP removal, respectively. For some experiments, MII eggs were collected from superovulated females at ~13 h after human chorionic gonadotropin injection as previously described (Gardner *et al.,* 2007). Zygotes were generated by in vitro fertilization as described (Gardner *et al.,* 2007). T_{eff} measurements of zygotes were taken at 90 min after insemination (ZP-free eggs were inseminated with 150,000 sperm/ml for 20 min, washed, and then cultured for 70 min).

Eggs were treated with 100 μg/ml concanavalin A (ConA; Sigma-Aldrich; diluted in Whitten's medium compatible buffer) for 30 min before and during T_{eff} measurement by MPA (see below). Treatment with the actin filament disruptor cytochalasin D (5 μg/ml; Calbiochem, Gibbstown, NJ) or the myosin light-chain kinase inhibitor ML-7 (15 μM; Calbiochem, La Jolla, CA; or Sigma-Aldrich) was done as previously described (McAvey *et al.,* 2002; Matson *et al.,* 2006) for 60 min before and during T_{eff} measurement by MPA. Controls were treated with a matching concentration of the solvent, DMSO. We also attempted to disrupt myosin-II activity with blebbistatin treatment, but found that this did not have consistent effects on T_{eff}. This may be linked with photoinactivation of blebbistatin (Kolega, 2004) and is consistent with a report that blebbistatin treatment did not have effects on first polar body emission (Schuh and Ellenberg, 2008).

T_{eff} Measurements by MPA

ZP-free oocytes, eggs, and zygotes were subjected to MPA using a motorized system (Effler *et al.,* 2006). Borosilicate capillaries (o.d., 1.0 mm, i.d., 0.75 mm; Sutter Instruments, Novato, CA) were pulled to an inner diameter of ~8 μm (PMP102 micropipette puller; MicroData Instruments, Woodhaven, NY) and broken on a microforge to smaller diameters; the average diameter of pipettes used here was 15 μm (range, 12–22 μm). Temperature of the culture medium for the T_{eff} measurements was maintained at 32–37°C with a miniature temperature controller (MTC; Bioscience Tools, San Diego, CA). Cells were measured in Whitten's medium containing 15 mM HEPES, 0.05% PVA, and, when needed, 5 μg/ml DAPI. The critical aspiration pressure (ΔP) that aspirated a tether length (L_p) that equaled the pipette radius (R_p) was measured (Figure 2B; Octtaviani *et al.,* 2006). The T_{eff} was calculated using the Law of Laplace ($\Delta p = 2T_{eff}(1/R_p - 1/R_c)$, where R_c is the radius of the cell outside the micropipette. All T_{eff} measurements were taken on microvillar regions of unfertilized and fertilized eggs unless otherwise noted, observing morphology and/or DAPI so that cortical regions over chromatin could be avoided. Phase contrast images of cells during MPA were captured using a 10× objective and a 1.6× optivar on an IX81 microscope equipped with MetaMorph software (Molecular Devices, Sunnyvale, CA). In a subset of the T_{eff} analyses of dominant-negative radixin (DN-RDX)-cRNA-injected eggs, injected cells with reduced T_{eff} measurements were recovered after MPA and subjected to immunofluorescence analysis with anti-cmyc and anti-phospho-ERM (pERM) antibodies (see below).

Dominant-Negative Disruption of ERM Function in Eggs

The region of encoding the N-terminal ERM association domain (NERMAD) of mouse radixin (amino acids 1-317) tagged with the c-myc epitope (EQKLISEEDLN) was cloned into pIVT plasmid (gift of Dr. Carmen Williams, NIEHS), and verified by DNA sequencing. This construct gives rise to the dominant-negative radixin with a cmyc epitope, which will be referred to as

DN-RDX. (A cmyc tag was used as we have been thus far unsuccessful in expressing a GFP-tagged version of the radixin N-terminal ERM association domain.) cRNA was synthesized from linearized pIVT-NERMAD using the mMessage Machine kit (Ambion, Austin, TX). cRNA (1 μg/μl) was injected using an Eppendorf FemtoJet injector on a Nikon TE2000-S inverted microscope (Melville, NY), with the oocytes in Whitten's medium containing 15 mM HEPES, 0.05% PVA, and 2.5 μM milrinone. After injection, oocytes were cultured in Whitten's medium containing 0.05% PVA and 2.5 μM milrinone for 3–7 h and then matured in vitro as described above. The term "DN-RDX-expressing eggs" refers the subset of cells that expressed detectable DN-RDX-cmyc and had reduced pERM.

Immunocytochemistry and Immunoblots

Oocytes and eggs were stained with the following primary antibodies: anti-phospho-myosin-II regulatory light chain (pMRLC; Cell Signaling Technology, Danvers, MA), anti-radixin (Sigma-Aldrich), anti-pERM (Cell Signaling Technology, Beverly, MA), or anti-β-tubulin (Invitrogen), or anti-α-tubulin (AA4.3; Developmental Studies Hybridoma Bank, University of Iowa, Department of Biology, Iowa City, IA), followed by secondary antibodies from Jackson ImmunoResearch (West Grove, PA). Sodium orthovanadate (100 μM; Sigma) was included for staining with the anti-pMRLC antibody. Fluorescently labeled phalloidin (Sigma-Aldrich) was used to stain actin. DNA was stained by mounting cells in Vectashield mounting medium (Vector Laboratories, Burlingame, CA) containing 1.5 μg/ml DAPI (Sigma-Aldrich). Images were collected using IPLab (Scanalytics, Fairfax, VA) or iVision (BioVision, Exton, PA) software.

Blots of protein lysates were probed with anti-ERM or anti-pERM (Cell Signaling Technology) or anti-radixin (Sigma), followed by goat anti-rabbit IgG conjugated to horseradish peroxidase (Jackson ImmunoResearch). ImageJ (http://rsb.info.nih.gov/ij/) was used to quantify band intensity.

Assessment of Soluble and Polymeric Actin in Oocytes and Eggs

Lysates of oocytes or eggs (200–250 per sample) were prepared in 25 μl of lysis buffer (50 mM NaCl, 1 mM $MgCl_2$, 1 mM EGTA, 10 mM HEPES, 1%

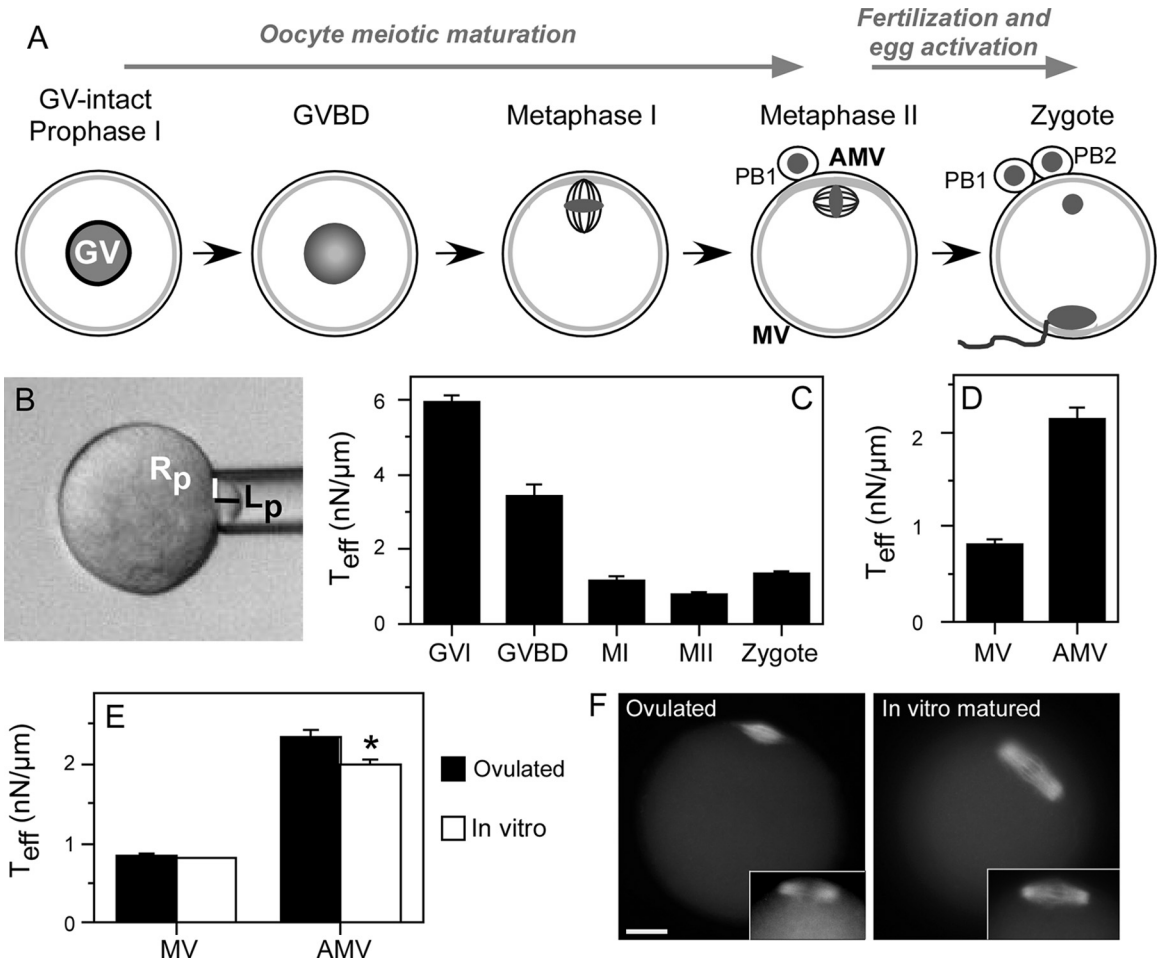

Figure 1. Changes in effective tension during meiotic maturation and fertilization. (A) Schematic diagram illustrating progression of the prophase I germinal vesicle-intact (GVI) oocytes through meiotic maturation, through germinal vesicle breakdown (GVBD) and metaphase I (MI) stages to metaphase II (MII) arrest, followed by fertilization-triggered exit from MII arrest. The MII egg is characterized by distinct domains of membrane and underlying cortex: the microvillar (MV) domain to which sperm bind and fuse, and the amicrovillar (AMV) domain, overlying the meiotic spindle and characterized by an actin-rich cap, contrasting the uniform distribution of actin and microvilli at prophase I stage. Gray lines indicate cortical actin. Polar bodies (PB1, first polar body; PB, second polar body) are the products of the asymmetric meiotic divisions. (B) Micropipette aspiration (MPA) of mouse eggs. The egg is aspirated until the equilibrium length of the cortex pulled into the pipette (L_p) equals the radius of the pipette (R_p). The aspiration pressure, where $L_p = R_p$, is defined as the critical pressure. (C) Effective tension (T_{eff}) in oocytes, eggs, and zygotes. For eggs and zygotes in this panel, assessments were done on microvillar domains. Number of cells analyzed: GVI, 142; GVBD, 16; MI, 16; MII, 387; and zygote, 46. (D) T_{eff})in MII eggs in the microvillar (MV) and amicrovillar (AMV) domains. These data are the composite of all cells analyzed: total MV, 387; total AMV, 175. (E) T_{eff} the microvillar (MV) and amicrovillar (AMV) domains of MII eggs that had been ovulated and matured in vivo (Ov) compared with eggs that had been matured to MII in vitro (IVM). Number of cells analyzed: ovulated MV, 200; ovulated AMV, 91; in vitro–matured MV, 187; in vitro–matured AMV, 84. (F) Spindle morphology, revealed by anti-tubulin staining, in ovulated and in vitro–matured M II eggs. Insets show a second example of a spindle in each type of egg. Scale bar, 15 μm.

Triton X-100, 1 μg/ml leupeptin, 1 μg/ml aprotinin, 0.1 mM AEBSF, 1 μM phalloidin). Lysates were centrifuged at 30,000 × *g* for 30 min, and the supernatant and pellet fractions were collected. These were probed by immunoblotting an anti-actin mAb (1 μg/ml, clone AC-40, Sigma-Aldrich), followed by peroxidase-conjugated anti-mouse IgG (Jackson ImmunoResearch). Detection was performed using a VersaDoc system with Quantity One software (Bio-Rad, Hercules, CA) to quantify band intensity.

Analysis of Fluorescence Staining of pERM and Actin in Eggs

Eggs were stained with anti-pERM antibodies (Cell Signaling Technology), or phalloidin to stain actin (Sigma-Aldrich; 25–100 ng/ml). Images were collected using IPLab (Scanalytics, Fairfax, VA) or iVision (BioVision, Exton, PA) software and analyzed using ImageJ (http://rsb.info.nih.gov/ij/). After background correction, integrated density measurements were taken of the entire cell (I_{whole}) using the elliptical selections tool to draw an ellipse around the cell. To measure the integrated density of the cytoplasmic region (I_{cyto}), the elliptical selections tool was used to draw an ellipse around only the cytoplasmic region of the cell, excluding the cortical region. I_{cyto} was subtracted from I_{whole} to obtain the integrated density of the cortical region (I_{cortex}). To verify the accuracy of this method, we also measured the intensities using the freehand tool to manually define the regions of interest in a subset of eggs. Both methods gave identical results; if the eggs were not completely symmetrical, the freehand tool was used.

RESULTS

The properties and functions of the membrane and cortex differ significantly in prophase I oocytes and MII eggs (Figure 1A). (Note: Throughout this article, the term "oocyte" will be used to refer to the female gamete generically and also for GVI, prophase I oocytes; the term "egg" connotes MII arrest.) Oocytes progress through meiotic maturation, characterized by progression through GVBD and MI, and then arrest at MII. Meiotic maturation in vivo occurs with ovulation and transit of the ovulated egg(s) to the oviduct; meiotic maturation can also occur in vitro, with the culture of prophase I oocytes in medium that supports a decrease in protein kinase A activity and the subsequent increase in CDK1 activity (Mehlmann, 2005). The MII egg is characterized by distinct domains of membrane and underlying cortex: the microvillar (MV) domain to which sperm bind and fuse, and the amicrovillar (AMV) domain, overlying the meiotic spindle and characterized by an actin-rich cap, contrasting the uniform distribution of actin and microvilli at prophase I stage (Figure 1A). Exit from MII is triggered by fertilization.

We hypothesized that the mechanical properties of oocytes would vary through these developmental transitions, given the changes that occur during meiosis and fertilization. T_{eff} measurements using MPA (Figure 1B) showed that as oocytes matured from prophase I (GVI) to MII, the effective tension varied about sixfold. GVI oocytes had a mean ± SEM T_{eff} value of 5.9 ± 0.2 nN/μm (Figure 1C, Figure S1), making oocytes among the more rigid cell types studied (Hochmuth, 2000). T_{eff} decreased through GVBD and metaphase I, reached a nadir at MII, and then increased after fertilization (Figures 1C, Figure S1). Interestingly, MII eggs were found to have mechanical polarity, with a nearly threefold difference in T_{eff} detected between the microvillar and amicrovillar domains (Figure 1D, Figure S1).

This work includes studies using injections of prophase I oocytes followed by in vitro maturation to MII, so we compared the T_{eff} levels in MII eggs that had been matured in vivo, with gonadotropin-induced ovulation, to the T_{eff} levels in eggs that had been matured in vitro. T_{eff} was not different between the microvillar domains of ovulated and in vitro matured eggs (ovulated, 0.84 ± 0.023 nN/μm [n = 200]; in vitro matured, 0.80 ± 0.018 nN/μm [n = 187]; Figure 1E, Figure S1). On the other hand, T_{eff} differed between the amicrovillar domains. Amicrovillar domains of ovulated eggs measured 2.3 ± 0.085 nN/μm (n = 91), and amicrovillar domains of in vitro matured eggs measured 2.0 ± 0.069 nN/μm (n = 84); this difference was statistically significant (p = 0.002) (Figure 1E, Figure S1). Because the MII spindle is sequestered in the amicrovillar domain, we used anti-tubulin staining to investigate if these differences in effective tension correlated with differences in the morphology of the MII spindle between ovulated eggs and in vitro matured eggs. Examples of these are shown in Figure 1F; spindles in ovulated eggs tended to be shorter and often with narrower poles, whereas spindles in in vitro matured eggs were longer with broader poles, consistent with other studies using similar in vitro maturation methods (Sanfins *et al.*, 2003, 2004; Barrett and Albertini, 2007); these references provide extensive characterization of spindle morphology in ovulated and in vitro–matured MII eggs.

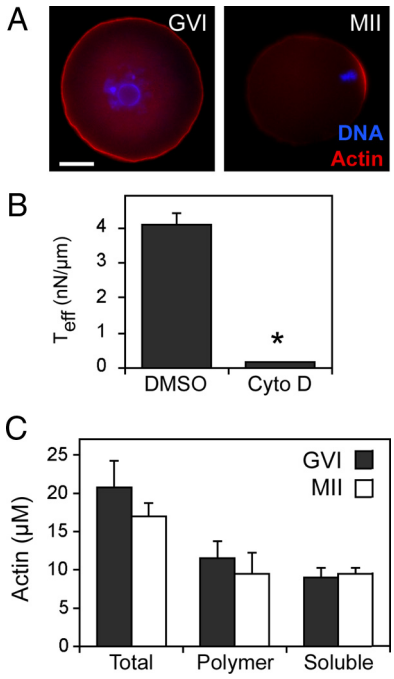

Figure 2. Effects of actin manipulation on oocyte effective tension. (A) Phalloidin staining of a GVI oocyte (left) and a metaphase II (MII) egg (right). Polarity develops during meiotic maturation, such that the metaphase II egg has an actin-rich cap over the meiotic spindle. Red, actin; blue, DNA. Scale bar, (left) 20 μm; (right) 22 μm. (B) Effects on effective tension (T_{eff}) of actin manipulation by cytochalasin D treatment of GVI oocytes (*p < 0.0001). Numbers of cells analyzed: cytochalasin D–treated GVI oocytes, 75; DMSO control GVI oocytes, 43. (C) Cellular concentration (in μM) of total actin, and actin in the phalloidin-stabilized, polymeric fraction (polymer) and in the soluble fraction in GVI oocytes (■) and MII eggs (□). Values for GVI oocytes show the mean ± range from two experiments and for MII eggs, mean ± range from three experiments.

The actin cytoskeleton plays a major role in cortical dynamics and tension in other cell types, and we show here that this is true for oocytes as well. Cytochalasin D treatment, which disrupts actin polymers, reduced T_{eff} in GVI oocytes by 95% (Figure 2B, Figure S2). Cytochalasin D–treated MII eggs were aspirated into the pipette once aspiration pressure was applied, making it impossible to obtain precise T_{eff} values but suggesting that these eggs had extremely low T_{eff}. Because of the sixfold difference in T_{eff} between oocytes and eggs, we hypothesized that actin levels would be higher in GVI oocytes as compared with MII eggs.

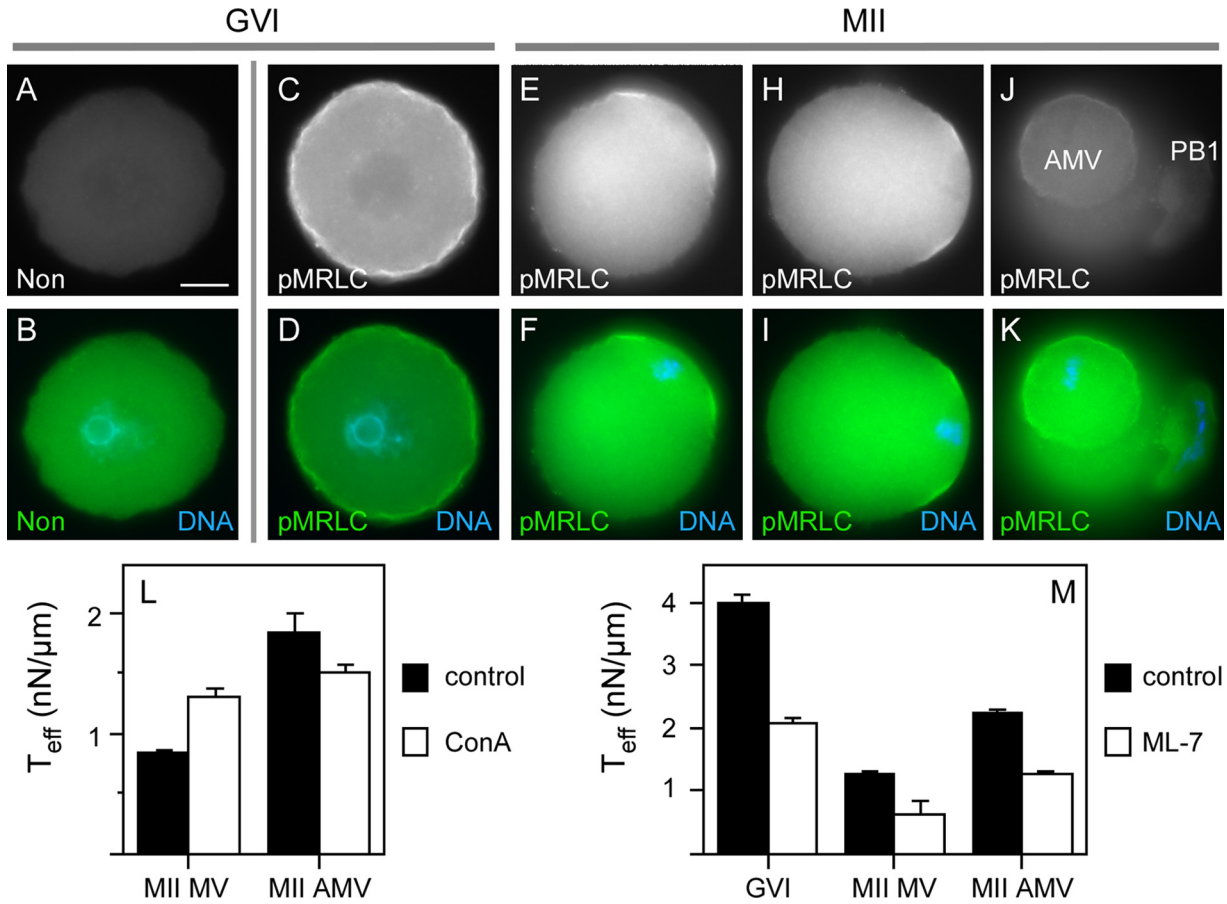

Figure 3. Localization of pMRLC and effects of myosin-II manipulation on effective tension. (A–K) Immunofluorescence localization of phosphorylated myosin-II regulatory light chain (pMRLC) in oocytes and eggs. Stages shown are GVI oocyte (A–D) and metaphase II (MII) eggs (E–K). With the exception of A and B (which show nonimmune antibody staining), the top row of black and white images shows pMRLC, whereas the second row of images shows pMRLC in green and DNA in blue. Images are taken at different focal planes; most are focused at or near the cell equator, whereas J and K are focused toward the top of the egg to show the amicrovillar domain (AMV). The egg in J and K also has the first polar body nearby (PB1). Scale bar, 20 μm. (L and M) Effects on effective tension (T_{eff}) of myosin manipulation by ConA treatment of MII egg microvillar domains (MV) and amicrovillar (AMV) domains (L) or ML-7-treatment on GVI oocytes (GVI), MII egg microvillar domains (MII MV), and MII egg amicrovillar domains (MII AMV; M). Values shown are mean T_{eff} ± SEM in nN/μm. ■, control values (medium for L, DMSO for M); □, T_{eff} values for treated eggs (ConA for L, 15 μM ML-7 for M). The difference between each control and treatment group is statistically significant (Mann Whitney U-test, $p < 0.05$). Number of cells analyzed: ConA-treated MII MV, 89; untreated MII MV controls, 61; ConA-treated MII AMV, 52; untreated MII AMV controls, 35; ML-7-treated GVI, 53; DMSO control GVI, 45; ML-7–treated-MII MV, 84; DMSO control MII MV, 79; ML-7–treated-MII AMV, 23; and DMSO control MII AMV, 36.

However, quantitative immunoblot analysis revealed that oocytes and eggs had comparable concentrations of total, polymeric, and soluble actin (Figure 2C), prompting us to consider additional tension-regulating factors to account for this T_{eff} difference between GVI oocytes and MII eggs.

Myosin-II contractility works with actin to mediate cortical tension in other cell types, and is regulated by phosphorylation of the myosin-II regulatory light chain. We find that the active, phosphorylated form of the myosin-II regulatory light chain (hereafter referred to as pMRLC) is detected in the oocyte/egg and is enriched in the cortex of oocytes and in the amicrovillar domain of eggs (Figure 3, A–K), colocalized with actin polymers (Figure 2A) and myosin-II heavy chains IIA and IIB (Maro *et al.*, 1984; Simerly *et al.*, 1998). The role of myosin-II in cortical tension and cell shape in mitotic cells has been characterized through manipulation of myosin-II–mediated contractility (Pasternak and Elson, 1985; Pasternak *et al.*, 1989; Lucero *et al.*, 2006; Kunda *et al.*, 2008); we used these methods to assess myosin-based mechanics in oocytes and eggs. Treatment of cells with concanavalin A (ConA) typically induces a myosin-II–dependent increase in cortical tension (Pasternak and Elson, 1985; Pasternak *et al.*, 1989; Kunda *et al.*, 2008). ConA-treated eggs showed an increase in T_{eff} in the microvillar domain compared with untreated controls (50%; $p < 0.001$, Mann-Whitney U-test) and a modest decrease in T_{eff} of the amicrovillar domain relative to controls (18%; $p = 0.14$, Mann-Whitney U-test; Figures 3L, Figure S3). These observations suggest that ConA treatment alters the normal mechanical polarity in MII eggs. The localizations of pMRLC and phosphorylated ERM (addressed below) were not dramatically different between controls and ConA-treated eggs (Figure S3).

Inhibition of myosin light-chain kinase (MLCK) activity with ML-7 affects cortical contractility in sea urchin zygotes (Lucero *et al.*, 2006) and alters certain events of mouse oocyte maturation and egg activation (Matson *et al.*, 2006; Li *et al.*, 2008a; Schuh and Ellenberg, 2008). We show that ML-7-treated oocytes and eggs had a ~50% decrease in T_{eff}; this decrease in T_{eff} in MII eggs was observed in both the microvillar and amicrovillar domains (Figures 3M, Figure S2).

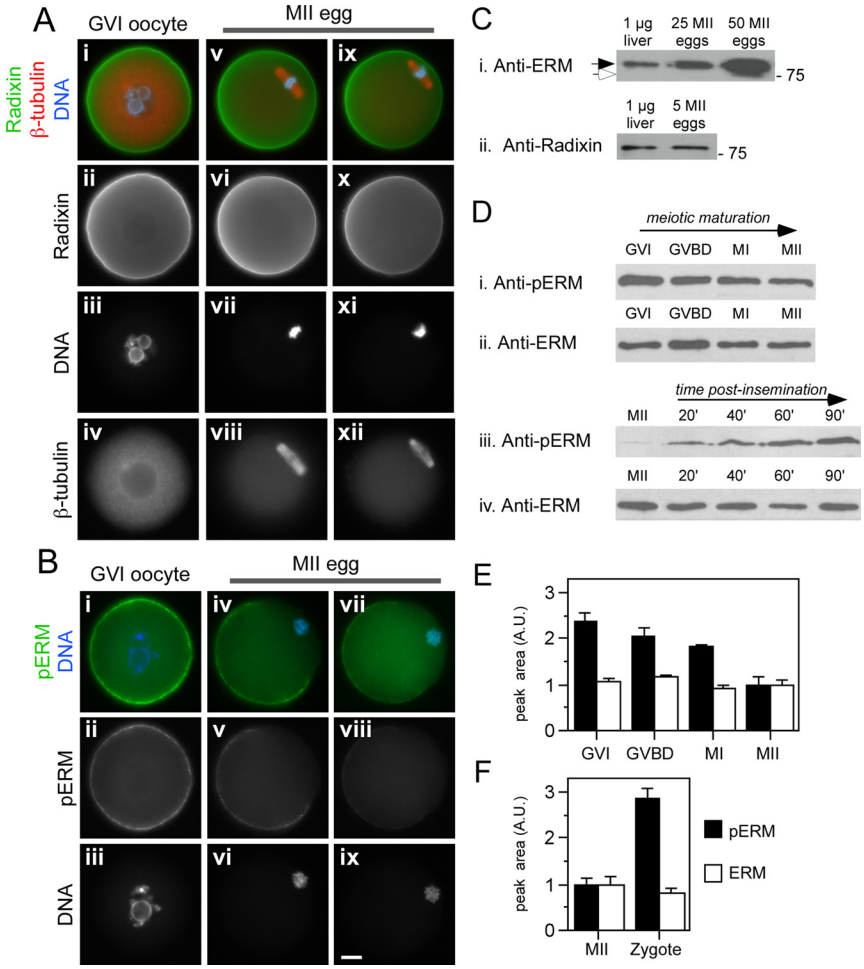

Figure 4. ERMs in mouse eggs. (A and B) Immunofluorescence analysis of radixin (A) and pERM (B) in GVI oocytes (Ai–iv; Bi–iii) and MII eggs (Av–xii and Biv–ix), showing anti-radixin (Aii, vi, and x), anti-pERM (Bii, v, and viii), DNA (Aiii, vii and xi and Biii, vi, and ix), or anti-β-tubulin (Aiv, viii, and xii). Scale bar, 15 μm. (C) Immunoblot analysis of ERM (i) or radixin (ii) expression in eggs. In Ci, the solid arrowhead indicates the electrophoretic mobility of ezrin and radixin, the open arrowhead indicates moesin. Radixin is detectable in lysates of five eggs (125 ng protein) with a band of comparable intensity to that detected in 1 μg of mouse liver lysate. (D) Representative blots of oocyte and egg lysates (20 cells per lane) probed with anti-pERM (i and iii) or anti-ERM (ii and iv) antibodies. Oocyte meiotic maturation (GVI to MII; i and ii) and fertilization (iii and iv) were analyzed in separate blots with different exposure times, to optimize capturing the range of signals (e.g., the blot in iii was exposed to show the increase in signal from unfertilized eggs to fertilized eggs). (E and F) Quantification of band intensities of anti-pERM (■) and ERM (□) levels during oocyte maturation (E) or the egg-to-embryo transition (F; zygote sample prepared at 90 min after insemination); sample blots are shown above in D. Values were normalized to metaphase II (MII) eggs.

These effects of ML-7 treatment suggest a connectedness of the cortical cytoskeleton as well as the fact that low concentrations of myosin II and/or low levels of myosin II activation (i.e., in the microvillar vs. amicrovillar domains, respectively) are sufficient to impact egg mechanics (Zhang and Robinson, 2005; Kunda *et al.*, 2008; Reichl *et al.*, 2008).

We next examined the ERM protein family. Moesin in *Drosophila* and enlazin, the closest ERM relative in *Dictyostelium*, contribute to cortical mechanics (Octtaviani *et al.*, 2006; Kunda *et al.*, 2008). Interestingly, radixin is very abundantly represented in the mouse oocyte transcriptome (e.g., Evsikov *et al.*, 2006; Unigene, www.BioGPS.org), but nothing is known of its function. We show here that mouse eggs express radixin and moesin (Figure 4, A–C), complementing reports of ezrin expression (Louvet *et al.*, 1996). Radixin is detectable in lysates of five eggs (125 ng protein) with a band of comparable intensity to that detected in 1 μg of mouse liver lysate (Figure 4Cii) and is present in the cortex of GVI oocytes and MII eggs (Figure 4A), in a localization similar to that observed for ezrin (Louvet *et al.*, 1996). The activity of ERMs is regulated by phosphorylation of a conserved threonine residue in the ERM C-terminal domain that stabilizes a conformation change that allows interactions with ligands, with actin filaments through the C-terminus domain and with the membrane through the FERM (4.1-ezrin-radixin-moesin) domain (Bretscher *et al.*, 2002; Niggli and Rossy, 2008; Fehon *et al.*, 2010). Active pERMs are localized to cortical regions of oocytes and eggs, with enrichment in the microvillar domain of eggs (Figure 4B). pERM levels decline during meiotic maturation to MII and then increase after fertilization (Figure 4, D–F), mirroring the changes in T_{eff} during these developmental transitions (Figure 1C).

ERM activity was disrupted through a dominant-negative approach (Skoudy *et al.*, 1999) by injecting oocytes with cRNA encoding the N-terminal ERM association domain of radixin tagged with the c-myc epitope, hereafter referred to as DN-RDX. Mouse ERM knockout studies show that there is significant functional redundancy between ezrin, radixin, and moesin (Doi *et al.*, 1999; Kikuchi *et al.*, 2002; Saotome *et al.*, 2004), providing strong rationale for a dominant-negative approach to perturb egg ERM function, because mouse eggs express all three ERM family members (Figure 4 and Louvet *et al.*, 1996). Staining with an anti-cmyc antibody showed that one-third of eggs injected with DN-RDX cRNA expressed detectable DN-RDX protein. This subset of eggs expressing DN-RDX protein had pERM levels reduced by 84% as determined by anti-pERM staining and analysis of the ratio of signal intensity in the cortex to the total signal intensity (I_{cortex}/I_{whole}; this was a way to normalize between individual eggs; Figure 5B). We also assessed cortical actin as a control and found that there was no difference in the I_{cortex}/I_{whole} of actin in uninjected, water-injected, or cRNA-injected eggs with decreased pERM (Figure 5B).

Effective tension levels were assessed in eggs injected with the DN-RDX cRNA and in control eggs (uninjected, water-injected). The entire population of DN-RDX–injected eggs

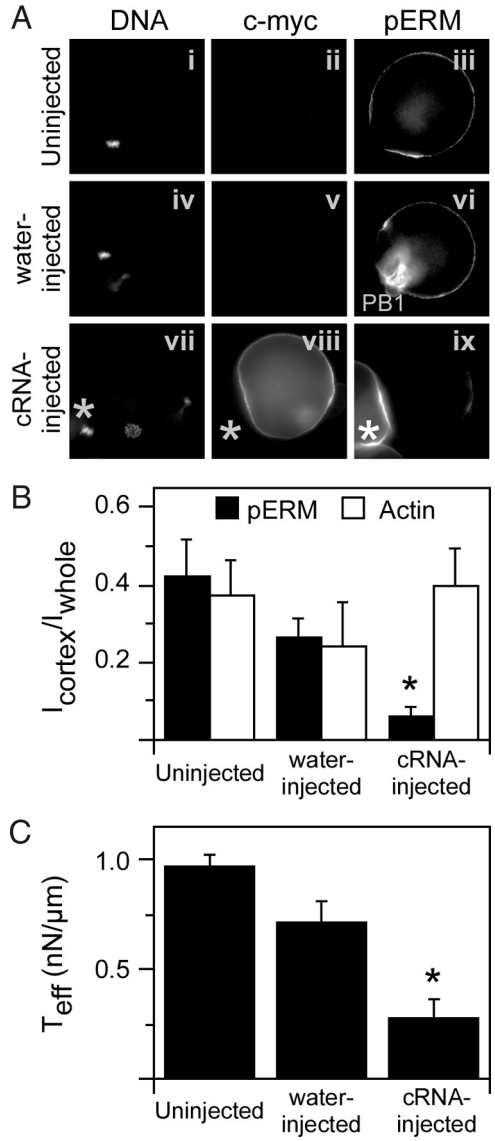

Figure 5. Perturbation of ERM action in eggs. (A) Analysis of DN-RDX-cmyc and pERM by immunofluorescence in uninjected (i–iii), water-injected (iv–vi), and DN-RDX-cRNA-injected eggs (vii–ix). DN-RDX-cmyc protein was detected in ~33% of eggs injected with DN-RDX-cmyc cRNA. (viii and ix) Two eggs, one with detectable cmyc staining (viii) and reduced pERM staining (ix), and a second egg (*) that does not have detectable cmyc staining (viii) and has cortically localized pERM (ix). (B) Assessment of pERM and actin levels in control (uninjected and water-injected) and DN-RDX–expressing egg through quantification of I_{cort}/I_{whole} signals (described in *Materials and Methods*). This analysis shows that cortical pERM (■) is reduced in DN-RDX–expressing eggs (*$p < 0.0001$), whereas the ratio of cortical/whole actin polymers is unaffected. Numbers of cells analyzed: uninjected, pERM, 5; uninjected actin, 8; water-injected, pERM, 4; water-injected, 4; cRNA-injected, pERM, 22; and cRNA-injected, actin, 14. (A sample of phalloidin staining of a metaphase II egg is shown in Figure 2.) (C) Effects of DN-RDX expression and reduction of pERM on effective tension (T_{eff}) levels in eggs. Eggs were subjected to T_{eff} measurements, then recovered, and analyzed for c-myc expression (indicative of DN-RDX expression) and reduction of pERM. Number of cells analyzed: uninjected, 10; water-injected, 7; and DN-RDX-expressing, 8. The difference between uninjected and water-injected eggs is not statistically significant, whereas the differences between the cRNA-injected eggs and the other two groups is significant (*$p < 0.001$). Furthermore, a small number of cRNA-injected eggs deformed as soon as aspiration pressure was applied, making it impossible to obtain a T_{eff} measurement but suggesting that these eggs had extremely low T_{eff}.

had a mean T_{eff} of 0.75 ± 0.048 nN/μm (Figure S2; $p = 0.16$; [Mann Whitney U-test] when these eggs were compared with the entire population of in vitro matured MII eggs [0.80 ± 0.018 nN/μm]), but this distribution in T_{eff} levels in DN-RDX–injected eggs is likely due to the fact that only about a third of these eggs express detectable DN-RDX protein. We were able to recover some eggs after the T_{eff} measurements and examine these for DN-RDX expression and reduction of pERM. The cRNA-injected eggs that had detectable DN-RDX protein, and reduced pERM levels had a mean T_{eff} 0.28 ± 0.085 nN/μM, which was significantly different from control eggs (Figure 5C, Figure S2). We also observed that a small number of DN-RDX–injected eggs deformed as soon as aspiration pressure was applied, similar to the cytochalasin D–treated eggs, suggesting that these eggs had extremely low T_{eff}.

We next sought to examine the biological effects associated with disrupted effective tension in eggs. Meiotic maturation and emission of the first polar body in DN-RDX cRNA-injected oocytes to MII appeared to occur normally. To determine if T_{eff} disruption affected function of MII egg function and the second meiotic division, we performed in vitro fertilization with control and DN-RDX–injected eggs as well as with cytochalasin D– and ML-7–treated eggs. These eggs could be fertilized but developed significant spindle abnormalities during exit from MII. In normal completion of meiosis II in control eggs (solvent [DMSO]-treated, uninjected, water-injected; Figure 6, A–C, J–M, and Q–T), the meiotic spindle elongates in anaphase II and then undergoes spindle rotation from its orientation parallel to the membrane. This rotation produces the second polar body, with the polar body developing from one of the chromatin-containing protrusions that forms before spindle rotation; the other protrusion resolves (Figure 6). Defects in second polar body emission and spindle rotation were observed in cytochalasin D– and ML-7–treated eggs, in agreement with previous studies (Maro *et al.*, 1984; Matson *et al.*, 2006); interestingly, spindle rotation failed in DN-RDX–expressing eggs but the spindle abnormalities differed from those in cytochalasin D– and ML-7–treated eggs. (Note: Polar body emission and spindle rotation appeared to be normal in ConA-treated eggs; see Figure S3 for details. This lack of an effect on polar body emission could be due to having to introduce ConA treatment after zygote creation, and/or due to the ConA-induced change in tension being insufficient to induce significant abnormalities during polar body emission.) In cytochalasin D–treated eggs, ML-7–treated eggs, and DN-RDX–expressing eggs, spindle elongation occurred but spindle rotation failed. The cytochalasin D–treated and ML-7–treated eggs arrested at this anaphase II-like stage and no polar body was formed, with only very modest protrusions over the chromatin (Figure 6, D–I; Maro *et al.*, 1984; Matson *et al.*, 2006). Fertilized DN-RDX–expressing eggs developed spindles that were distorted and curved; a pair of extended polar body-like structures was associated with the chromatin at the ends of these distorted spindles (Figure 6, N–P). These PB-like structures did not resolve, still persisting at 4 h after inseminations (Figure 6, U-BB).

DISCUSSION

Cellular mechanics are a critical determinant governing the cell shape changes that occur as the cell progresses through the cell cycle (Reichl *et al.*, 2005; Pollard, 2009). Cell morphogenesis during mitosis and many other processes is the result of an intricate interplay between three elements—biochemistry, mechanics, morphology—each of which is

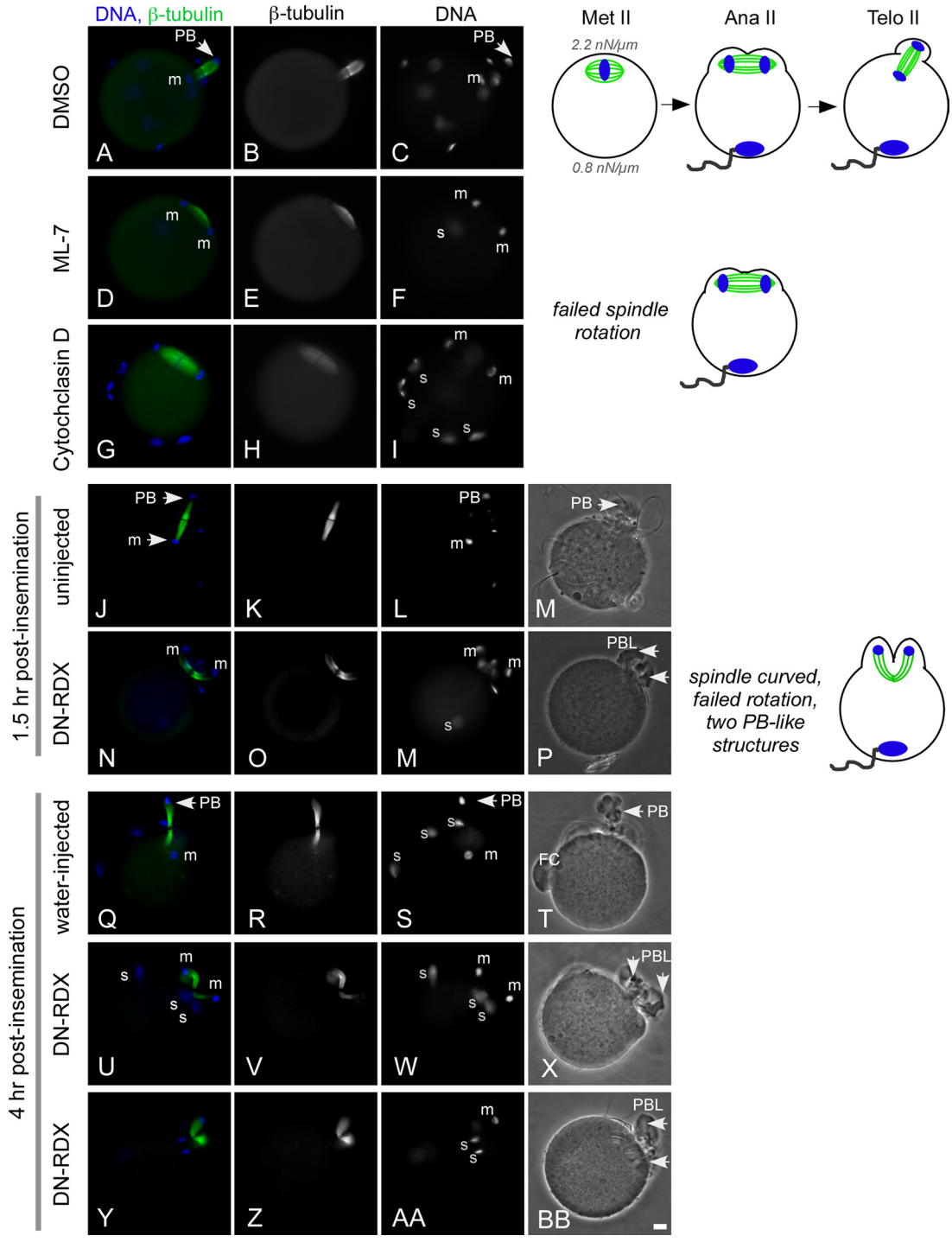

Figure 6. Spindle defects upon exit from metaphase II arrest with actin, myosin-II, or ERM disruption. Eggs were inseminated for 1.5 h (A–P) or 4 h (Q-BB). Control fertilized eggs (A–C, J–M, and Q–T) show normal spindle rotation and second polar body morphology, as illustrated in the schematic diagram. A failure in spindle rotation was observed in eggs treated with the MLCK inhibitor ML-7 (D–F; 73/75 eggs) and in eggs treated with the actin filament disruptor cytochalasin D (G–I; 34/34 eggs). Distorted, curved spindles were observed in DN-RDX–expressing eggs (N–P, U-BB; 26/36 eggs). In these embryos, two polar body-like (PBL) structures formed; these PBL structures did not resolve with increased time after insemination (U-BB). Arrowheads identify polar bodies (PB) and PBL structures. Maternal DNA is labeled m, and sperm DNA is labeled s; some eggs are polyspermic, although this is not uncommon with the insemination conditions used, particularly with cytochalasin D–treated eggs (McAvey *et al.*, 2002). In several panels, DNA of the fertilizing sperm is out of the plane of focus. FC (T) identifies the fertilization cone containing the DNA of a fertilizing sperm. Scale bar, (DD) 10 μm.

inextricably linked with the other. Biochemistry clearly influences morphology and mechanics, whereas less intuitively but just as significantly, morphology and mechanics also can influence biochemistry (Zhang and Robinson, 2005; Ren *et al.*, 2009). These three elements work to dictate dramatic cell shape changes such as during mitosis (Reichl *et al.*,

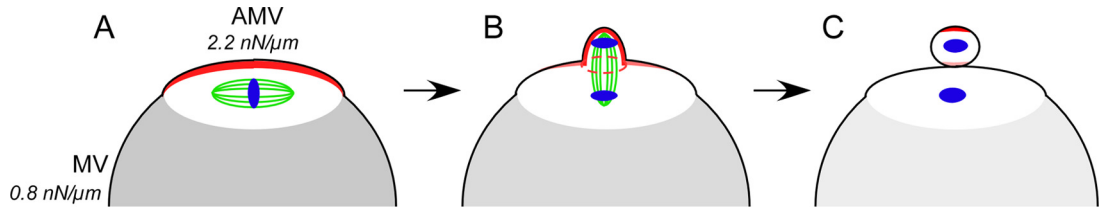

Figure 7. Schematic diagram of mechanical properties in the egg driving asymmetric cell division. (A) The mechanical polarity in the metaphase II (MII) mouse egg between the microvillar domain (MV) and the actin- and myosin-II–enriched (red) amicrovillar domain over the spindle (AMV); the amicrovillar domain creates a microdomain in the egg containing the metaphase II spindle (green). The subregion of the egg cell defined by the amicrovillar domain with its increased local T_{eff} likely serves to isolate the spindle and developing polar body and allows contraction mediated by actin and myosin-II (red) to locally deform the cortex. Myosin II accumulates at the polar cortex of the emerging polar body (B), facilitating asymmetric meiotic cell division (C). The change in gray shading in the cytoplasm through A–C illustrates the progression of the egg from the metaphase II arrest (A) through anaphase and telophase to embryonic interphase.

2005). Asymmetric cell divisions present unique challenges (Gönczy, 2008), and the mouse egg is an especially interesting case. The mouse egg undergoes a highly asymmetric cell division after an extended MII arrest, and yet maintains a relatively simple, largely spherical, cell morphology. Thus, in the case of the mouse egg, cell morphology does not change significantly, but the other two elements, biochemistry and mechanics, do change. There are detectable redistributions of actin, myosin-II, and ERM proteins (changes in local biochemistry) and a major modulation of effective tension. An approximately sixfold decrease in effective tension occurs as oocytes progress from prophase I to MII, and then a ~1.5-fold increase occurs with MII exit and the egg-to-embryo transition. Known parameters that affect cellular mechanics include actin concentration and polymer length, cross-linking proteins, and myosin mechanochemistry. We find that actin is central to the mechanics of mouse eggs and that myosin-II and ERMs contribute about twice of the effective tension. This is consistent with reported contributions of actin-associated proteins to cortical mechanics (e.g., myosin-II and Rac have up to about threefold effects on mechanics in *Dictyostelium* cells; Gerald *et al.*, 1998; Girard *et al.*, 2004; Zhang and Robinson, 2005; Octtaviani *et al.*, 2006; Kunda *et al.*, 2008; Reichl *et al.*, 2008).

We have also discovered a new aspect of cell polarity in the MII-arrested egg, as we find there is a ~2.5-fold mechanical tension differential between amicrovillar and microvillar domains. These two domains have well-characterized differences in morphology, molecular composition and functionality (Nicosia *et al.*, 1977; Brunet and Maro, 2005; Azoury *et al.*, 2008), with sperm-egg fusion occurring on the microvillar domain and the meiotic spindle being sequestered in the amicrovillar domain. The lower tension in the microvillar domain of the mouse egg does not seem to be a contributing factor to sperm fusion occurring preferentially in this region, nor does the increased tension in the zygote appear to be the foundation of the membrane block to polyspermy (Gardner and Evans, 2006), as even higher tension is present in GVI oocytes and these cells can be fertilized by sperm. The tension in the egg, instead, appears to be critical for meiotic spindle function. These mechanical properties of the egg are regulated by myosin-II, enriched in the amicrovillar domain, and pERM, enriched in the microvillar domain, and disruption of actin, myosin-II, or pERM function is associated with spindle defects with exit from MII upon fertilization. This work reveals an entirely new function for the egg cytoskeleton, in addition to its appreciated roles in spindle positioning (Maro *et al.*, 1984; Longo, 1987; Simerly *et al.*, 1998; Matson *et al.*, 2006; Azoury *et al.*, 2008; Li *et al.*, 2008a; Schuh and Ellenberg, 2008), establishment of the cortical endoplasmic reticulum during meiotic maturation (FitzHarris *et al.*, 2007), and organization of a subcortical complex that appears to be critical for progression to early cleavage stages of development (Li *et al.*, 2008b; Yurttas *et al.*, 2008).

The discovery of this ~2.5-fold mechanical differential between the microvillar and amicrovillar domains in mouse eggs sheds important light on asymmetric cell division. The mechanics that produce symmetrically sized daughter cells are coming into view, with evidence for fluid-like (i.e., Laplace-like) pressures contributing alongside myosin-II–generated contractility to drive furrow ingression (Zhang and Robinson, 2005; Reichl *et al.*, 2008). The results presented here suggest that the egg prepares for second polar body emission during MII arrest by establishing at MII a rigid "cytoskeletal plaque" enriched in actin and myosin-II (i.e., the amicrovillar domain; Figure 7). The amicrovillar domain then serves to isolate the MII spindle and then the developing polar body from the rest of the egg; this in turn allows myosin-II–mediated contraction to deform the cortex in this specific region, facilitating asymmetric cell division (Figure 7). Interestingly, we observe a difference in T_{eff} in the amicrovillar domains of ovulated eggs and in vitro matured eggs, which also have differences in spindle morphology (Sanfins *et al.*, 2003; Barrett and Albertini, 2007). This difference in amicrovillar T_{eff} may be a mechanistic factor associated with these spindle morphology differences, combined with γ-tubulin distribution, which has also been associated with the spindle size differences observed between ovulated and in vitro–matured eggs (Barrett and Albertini, 2007). Additional studies are required, of course, to flesh out the implications of this for cytokinesis, but these observations provide an important starting point. This work is the first report of the mechanical properties in mammalian oocytes, how they impact processes such as spindle rotation, and what the molecular underpinnings of these mechanics are. The coordinated action of cytoskeletal proteins is at work during cytokinesis in *Dictyostelium*, with actin cross-linkers, including enlazin, mediating resistive stresses that control myosin-II–dependent stress generation in the furrow region (Zhang and Robinson, 2005; Reichl *et al.*, 2008). It is intriguing to speculate that similar forces, such as pERM providing a resistive function to balance myosin-II contractility in the amicrovillar domain, direct morphological changes in the mouse egg. In addition to expanding our understanding of the functions of the egg cortex, these results provide significant insights into how mechanical factors are at work for a very asymmetric, meiotic cell division.

ACKNOWLEDGMENTS

We thank Carmen Williams (NIEHS; Research Triangle Park, NC) for the pIVT plasmid and Amelia Mackenzie for one of the images of the anti-tubulin–stained ovulated eggs. This work was supported by the National Institutes of Health Grants GM066817 to D.N.R. and HD037696 and HD045671 to J.P.E. and the March of Dimes Grant 6-FY-04-59 to J.P.E.

REFERENCES

Azoury, J., Lee, K. W., Georget, V., Rassinier, P., Leader, B., and Verlhac, M. H. (2008). Spindle positioning in mouse oocytes relies on a dynamic meshwork of actin filaments. Curr. Biol. *18*, 1514–1519.

Barrett, S. L., and Albertini, D. F. (2007). Allocation of gamma-tubulin between oocyte cortex and meiotic spindle influences asymmetric cytokinesis in the mouse oocyte. Biol. Reprod. *76*, 949–957.

Bretscher, A., Edwards, K., and Fehon, R. G. (2002). ERM proteins and merlin: integrators at the cell cortex. Nat. Rev. Mol. Cell Biol. *3*, 586–599.

Brunet, S., and Maro, B. (2005). Cytoskeleton and cell cycle control during meiotic maturation of the mouse oocyte: integrating time and space. Reproduction *130*, 801–811.

Carreno, S., Kouranti, I., Glusman, E. S., Fuller, M. T., Echard, A., and Payre, F. (2008). Moesin and its activating kinase Slik are required for cortical stability and microtubule organization in mitotic cells. J. Cell Biol. *180*, 739–746.

Cheng, K.C.-C., Klancer, R., Singson, A., and Seydoux, G. (2009). Regulation of MBK-2/DYRK by CDK-1 and the pseudophosphatases EGG-4 and EGG-5 during the oocyte-to-embryo transition. Cell *139*, 560–572.

Cho, W. K., Stern, S., and Biggers, J. D. (1974). Inhibitory effect of dibutyryl cAMP on mouse oocyte maturation in vitro. J. Exp. Zool. *187*, 383–386.

Cole, K. S. (1932). Surface forces of the *Arbacia* egg. J. Cell Comp. Physiol. *1*, 1–9.

Cole, K. S., and Michaelis, E. M. (1932). Surface forces of fertilized Arbacia eggs. J. Cell Comp. Physiol. *2*, 121–126.

Deng, M., Suraneni, P., Schultz, R. M., and Li, R. (2007). The Ran GTPase mediates chromatin signaling to control cortical polarity during polar body extrusion in mouse oocytes. Dev. Cell *12*, 301–308.

Derganc, J., Božic, B., Sventina, S., and Žekš, B. (2000). Stability analysis of micropipette aspriation of neutrophils. Biophys. J. *79*, 153–162.

Doi, Y., Itoh, M., Yonemura, S., Ishihara, S., Takano, H., Noda, T., and Tsukita, S. (1999). Normal development of mice and unimpaired cell adhesion/cell motility/actin-based cytoskeleton without compensatory up-regulation of ezrin or radixin in moesin gene knockout. J. Biol. Chem. *274*, 2315–2321.

Effler, J. C., Kee, Y. S., Berk, J. M., Tran, M. N., Iglesias, P. A., and Robinson, D. N. (2006). Mitosis-specific mechanosensing and contractile-protein redistribution control cell shape. Curr. Biol. *16*, 1962–1967.

Esposito, G., Vitale, A. M., Leijten, F. P., Strik, A. M., Koonen-Reemst, A. M., Yurttas, P., Robben, T. J., Coonrod, S., and Gossen, J. A. (2007). Peptidylarginine deiminase (PAD) 6 is essential for oocyte cytoskeletal sheet formation and female fertility. Mol. Cell. Endocrinol. *273*, 25–31.

Evans, J. P., Foster, J. A., McAvey, B. A., Gerton, G. L., Kopf, G. S., and Schultz, R. M. (2000). The effects of perturbation of cell polarity on molecular markers of sperm-egg binding sites on mouse eggs. Biol. Reprod. *62*, 76–84.

Evsikov, A. V., Graber, J. H., Brockman, J. M., Hampl, A., Holbrook, A. E., Singh, P., Eppig, J. J., Solter, D., and Knowles, B. B. (2006). Cracking the egg: molecular dynamics and evolutionary aspects of the transition from the fully grown oocyte to embryo. Genes Dev. *20*, 2713–2727.

Fehon, R. G., McClatchey, A. I., and Bretscher, A. (2010). Organizing the cell cortex: the role of ERM proteins. Nat. Rev. Mol. Cell Biol. *11*, 276–287.

FitzHarris, G., Marangos, P., and Carroll, J. (2007). Changes in endoplasmic reticulum structure during mouse oocyte maturation are controlled by the cytoskeleton and cytoplasmic dynein. Dev. Biol. *305*, 133–144.

Gardner, A. J., and Evans, J. P. (2006). Mammalian membrane block to polyspermy: new insights into how mammalian eggs prevent fertilisation by multiple sperm. Reprod. Fertil. Dev. *18*, 53–61.

Gardner, A. J., Williams, C. J., and Evans, J. P. (2007). Establishment of the mammalian membrane block to polyspermy: Evidence for calcium-dependent and -independent regulation. Reproduction *133*, 383–393.

Gerald, N., Dai, J., Ting-Beall, H. P., and De Lozanne, A. (1998). A role for *Dictyostelium* racE in cortical tension and cleavage furrow progression. J. Cell Biol. *141*, 483–492.

Girard, K. D., Chaney, C., Delannoy, M., Kuo, S. C., and Robinson, D. N. (2004). Dynacortin contributes to cortical viscoelasticity and helps define the shape changes of cytokinesis. EMBO J. *23*, 1536–1546.

Gönczy, P. (2008). Mechanisms of asymmetric cell division: flies and worms pave the way. Nat. Rev. Mol. Cell Biol. *9*, 355–366.

Halet, G., and Carroll, J. (2007). Rac activity is polarized and regulates meiotic spindle stability and anchoring in mammalian oocytes. Dev. Cell *12*, 309–317.

Harvey, E. N., and Fankhauser, G. (1933). The tension at the surface of the eggs of the salamander, *Triturus* (*Diemyctylus*) *viridescens*. J. Cell Comp. Physiol. *3*, 463–475.

Hassold, T., and Hunt, P. (2001). To err (meiotically) is human: the genesis of human aneuploidy. Nat. Rev. Genet *2*, 280–291.

Hiramoto, Y. (1976). Mechanical properties of starfish oocytes. Dev. Growth Differ *20*, 205–209.

Hochmuth, R. M. (2000). Micropipet aspiration of living cells. J. Biomech. *33*, 15–22.

Jankovics, F., Sinka, R., Lukacsovich, T., and Erdelyi, M. (2002). MOESIN crosslinks actin and cell membrane in *Drosophila* oocytes and is required for OSKAR anchoring. Curr. Biol. *12*, 2060–2065.

Kikuchi, S., Hata, M., Fukumoto, K., Yamane, Y., Matsui, T., Tamura, A., Yonemura, S., Yamagishi, H., Keppler, D., and Tsukita, S. (2002). Radixin deficiency causes conjugated hyperbilirubinemia with loss of Mrp2 from bile canalicular membranes. Nat. Genet. *31*, 320–325.

Kolega, J. (2004). Phototoxicity and photoinactivation of blebbistatin in UV and visible light. Biochem. Biophys. Res. Commun. *320*, 1020–1025.

Kunda, P., Pelling, A. E., Liu, T., and Baum, B. (2008). Moesin controls cortical rigidity, cell rounding, and spindle morphogenesis during mitosis. Curr. Biol. *18*, 91–101.

Leader, B., Lim, H., Carabatsos, M. J., Harrington, A., Ecsedy, J., Pellman, D., Maas, R., and Leder, P. (2002). Formin-2, polyploidy, hypofertility and positioning of the meiotic spindle in mouse oocytes. Nat. Cell Biol. *4*, 921–928.

Li, H., Guo, F., Rubinstein, B., and Li, R. (2008a). Actin-driven chromosomal motility leads to symmetry breaking in mammalian meiotic oocytes. Nat. Cell Biol. *10*, 1301–1308.

Li, L., Baibakov, B., and Dean, J. (2008b). A subcortical maternal complex essential for preimplantation mouse embryogenesis. Dev. Cell *15*, 416–425.

Longo, F. J. (1987). Actin-plasma membrane associations in mouse eggs and oocytes. J. Exp. Zool. *243*, 29–322.

Louvet, S., Aghion, J., Santa-Maria, A., Mangeat, P., and Maro, B. (1996). Ezrin becomes restricted to outer cells following asymmetrical division in the preimplantation mouse embryo. Dev. Biol. *177*, 568–579.

Lucero, A., Stack, C., Bresnick, A. R., and Shuster, C. B. (2006). A global, myosin light chain kinase-dependent increase in myosin II contractility accompanies the metaphase-anaphase transition in sea urchin eggs. Mol. Biol. Cell *17*, 4093–4104.

Maro, B. B., Johnson, M. H., Pickering, S. J., and Flach, G. (1984). Changes in actin distribution during fertilization of the mouse egg. J. Embryol. Exp. Morph. *81*, 211–237.

Maruyama, R. *et al.* (2007). EGG-3 regulates cell-surface and cortex rearrangements during egg activation in *Caenorhabditis elegans*. Curr. Biol. *17*, 1555–1560.

Matson, S., Markoulaki, S., and Ducibella, T. (2006). Antagonists of myosin light chain kinase and of myosin II inhibit specific events of egg activation in fertilized mouse eggs. Biol. Reprod. *74*, 169–176.

McAvey, B. A., Wortzman, G. B., Williams, C. J., and Evans, J. P. (2002). Involvement of calcium signaling and the actin cytoskeleton in the membrane block to polyspermy in mouse eggs. Biol. Reprod. *67*, 1342–1352.

Mehlmann, L. M. (2005). Stops and starts in mammalian oocytes: recent advances in understanding the regulation of meiotic arrest and oocyte maturation. Reproduction *130*, 791–799.

Mitchison, J. M., and Swann, M. M. (1954). The mechanical properties of the cell surface: II. The unfertilized sea-urchin egg. J. Exp. Biol. *31*, 461–472.

Mitchison, J. M., and Swann, M. M. (1955). The mechanical properties of the cell surface: III. The sea-urchin egg from fertilization to cleavage. J. Exp. Biol. *32*, 734–750.

Na, J., and Zernicka-Goetz, M. (2006). Asymmetric positioning and organization of the meiotic spindle of mouse oocytes requires CDC42 function. Curr. Biol. *16*, 1249–1254.

Nakamura, S., and Hiramoto, Y. (1978). Mechanical properties of the cell surface in starfish eggs. Dev. Growth Differ. *20*, 317–327.

Nicosia, S. V., Wolf, D. P., and Inoue, M. (1977). Cortical granule distribution and cell surface characteristics in mouse eggs. Dev. Biol. *57*, 56–74.

Niggli, V., and Rossy, J. (2008). Ezrin/radixin/moesin: versatile controllers of signaling molecules and of the cortical cytoskeleton. Int J Biochem. Cell Biol. *40*, 344–349.

Octtaviani, E., Effler, J. C., and Robinson, D. N. (2006). Enlazin, a natural fusion of two classes of canonical cytoskeletal proteins, contributes to cytokinesis dynamics. Mol. Biol. Cell *17*, 5275–5286.

Parry, J. M. *et al.* (2009). EGG-4 and EGG-5 link events of the oocyte-to-embryo transition with meiotic progression in *C. elegans.* Curr. Biol. *19*, 1752–1757.

Pasternak, C., and Elson, E. L. (1985). Lymphocyte mechanical response triggered by cross-linking surface receptors. J. Cell Biol. *100*, 860–872.

Pasternak, C., Spudich, J. A., and Elson, E. L. (1989). Capping of surface receptors and concomitant cortical tension are generated by conventional myosin. Nature *341*, 549–551.

Polesello, C., Delon, I., Valenti, P., Ferrer, P., and Payre, F. (2002). Dmoesin controls actin-based cell shape and polarity during *Drosophila melanogaster* oogenesis. Nat. Cell Biol. *4*, 782–789.

Pollard, T. D. (2009). Mechanics of cytokinesis in eukaryotes. Curr. Opin. Cell Biol. *22*, 50–56.

Rappaport, R. (1967). Cell division: direct measurement of maximum tension exerted by furrow of echinoderm eggs. Science *156*, 1241–1243.

Reichl, E. M., Effler, J. C., and Robinson, D. N. (2005). The stress and strain of cytokinesis. Trends Cell Biol. *15*, 200–206.

Reichl, E. M., Ren, Y., Morphew, M. K., Delannoy, M., Effler, J. C., Girard, K. D., Divi, S., Iglesias, P. A., Kuo, S. C., and Robinson, D. N. (2008). Interactions between myosin and actin crosslinkers control cytokinesis contractility dynamics and mechanics. Curr. Biol. *18*, 471–480.

Ren, Y., Effler, J. C., Norstrome, M., Luo, T., Firtel, R. A., Iglesias, P. A., Rock, R. S., and Robinson, D. N. (2009). Mechanosensing through cooperative interactions between myosin II and the actin crosslinker cortexillin. Curr. Biol. *19*, 1421–1428.

Sanfins, A., Lee, G. Y., Plancha, C. E., Overstrom, E. W., and Albertini, D. F. (2003). Distinctions in meiotic spindle structure and assembly during in vitro and in vivo maturation of mouse oocytes. Biol. Reprod. *69*, 2059–2067.

Sanfins, A., Plancha, C. E., Overstrom, E. W., and Albertini, D. F. (2004). Meiotic spindle morphogenesis in in vivo and in vitro matured mouse oocytes: insights into the relationship between nuclear and cytoplasmic quality. Hum. Reprod. *19*, 2889–2899.

Saotome, I., Curto, M., and McClatchey, A. I. (2004). Ezrin is essential for epithelial organization and villus morphogenesis in the developing intestine. Dev. Cell *6*, 855–864.

Sardet, C., Prodon, F., Dumollard, R., Chang, P., and Chenevert, J. (2002). Structure and function of the egg cortex from oogenesis through fertilization. Dev. Biol. *241*, 1–23.

Sawai, T., and Yoneda, M. (1974). Wave of stiffness propagating along the surface of the newt egg during cleavage. J. Cell Biol. *60*, 1–7.

Schuh, M., and Ellenberg, J. (2008). A new model for asymmetric spindle positioning in mouse oocytes. Curr. Biol. *18*, 1986–1992.

Selman, G. G., and Waddington, C. H. (1955). The mechanism of cell division in the cleavage of the newt's egg. J. Exp. Biol. *32*, 700–733.

Simerly, C., Nowak, G., de Lanerolle, P., and Schatten, G. (1998). Differential expression and functions of cortical myosin IIA and IIB isotypes during meiotic maturation, fertilization, and mitosis in mouse oocytes and embryos. Mol. Biol. Cell *9*, 2509–2525.

Skoudy, A., Nhieu, G. T., Mantis, N., Arpin, M., Mounier, J., Gounon, P., and Sansonetti, P. (1999). A functional role for ezrin during *Shigella flexneri* entry into epithelial cells. J. Cell Sci. *112*, 2059–2068.

Stitzel, M. L., Cheng, K. C., and Seydoux, G. (2007). Regulation of MBK-2/Dyrk kinase by dynamic cortical anchoring during the oocyte-to-zygote transition. Curr. Biol. *17*, 1545–1554.

Tsafriri, A., Chun, S. Y., Zhang, R., Hsueh, A.J.W., and Conti, M. (1996). Oocyte maturation involves compartmentalization and opposing changes of cAMP levels in follicular somatic and germ cells: Studies using selective phosphodiesterase inhibitors. Dev. Biol. *178*, 393–402.

Whitten, W. K. (1971). Nutrient requirements for the culture of preimplantation embryos in vitro. Adv. Biosci. *6*, 129–139.

Wolpert, L. (1966). The mechanical properties of the membrane of the sea urchin egg during cleavage. Exp. Cell Res. *41*, 385–396.

Yurttas, P., Vitale, A. M., Fitzhenry, R. J., Cohen-Gould, L., Wu, W., Gossen, J. A., and Coonrod, S. A. (2008). Role for PADI6 and the cytoplasmic lattices in ribosomal storage in oocytes and translational control in the early mouse embryo. Development *135*, 2627–2636.

Zhang, W., and Robinson, D. N. (2005). Balance of actively generated contractile and resistive forces controls cytokinesis dynamics. Proc. Natl. Acad. Sci. USA *102*, 7186–7191.

Cortical mechanics and meiosis II completion in mammalian oocytes are mediated by myosin-II and ezrin-radixin-moesin (ERM) proteins

- SUPPLEMENT –

Three supplemental data figures and legends

Stephanie M. Larson[1] *, Hyo J. Lee[1]*, Pei-hsuan Hung[1], Lauren M. Matthews[1], Douglas N. Robinson[2,3] **, and Janice P. Evans[1] **

[1] Department of Biochemistry and Molecular Biology, Bloomberg School of Public Health, and [2] Department of Cell Biology and [3] Department of Pharmacology and Molecular Sciences, School of Medicine; Johns Hopkins University, Baltimore, Maryland

* These authors contributed equally.

** Corresponding authors (dnr@jhmi.edu, jpevans@jhsph.edu)

Address for correspondence:
Janice P. Evans
Department of Biochemistry and Molecular Biology
Bloomberg School of Public Health
Johns Hopkins University
615 N. Wolfe St.
Baltimore, MD 21205
jpevans@jhsph.edu
Telephone: 410-614-5557
Fax: 410-614-2356

FIGURE LEGENDS FOR SUPPLEMENTAL FIGURES

Supplemental Figure 1

Frequency distributions of effective tension measurements in oocytes, eggs, and zygotes

These histograms correspond to the data presented in Figure 1C and D. Each graph is a frequency distribution, with the x-axis indicating T_{eff} (in nN/μm) and the y-axis indicating the number of cells with the indicated T_{eff}. Values shown for each group are the mean ± SEM. Panel A shows comparisons of T_{eff} changes through meiosis, with the same scale on the x-axes: GV-intact (GVI, n = 142), germinal vesicle breakdown (GVBD, n = 16), metaphase I (MI, n = 16), metaphase II (MII, n = 387; ovulated and *in vitro* matured), and zygote (n = 46). The differences between T_{eff} measurements of each stage in this series are statistically significantly different (Mann Whitney U-test, $p < 0.05$). Panels B and C show T_{eff} measurements from metaphase II eggs, with the same scale on the x-axes: microvillar domain of all MII eggs (MII MV, n = 387), amicrovillar domain of all MII eggs (MII AMV, n = 175), microvillar domain of ovulated MII eggs (n = 200), and microvillar domain of *in vitro* matured MII eggs (MII IVM, n = 187), amicrovillar domain of ovulated MII eggs (n = 91), and amicrovillar domain of *in vitro* matured MII eggs (MII IVM, n = 84). The difference between T_{eff} measurements of the microvillar and amicrovillar domains of metaphase II eggs is statistically significantly (Mann-Whitney U test, $p < 0.0001$). Ovulated (*in vivo* matured) eggs and *in vitro* matured eggs have identical tension levels in the microvillar domains, whereas the T_{eff} levels of the amicrovillar domains between ovulated and *in vitro* matured eggs are statistically significantly different (Mann-Whitney U test, $p = 0.01$).

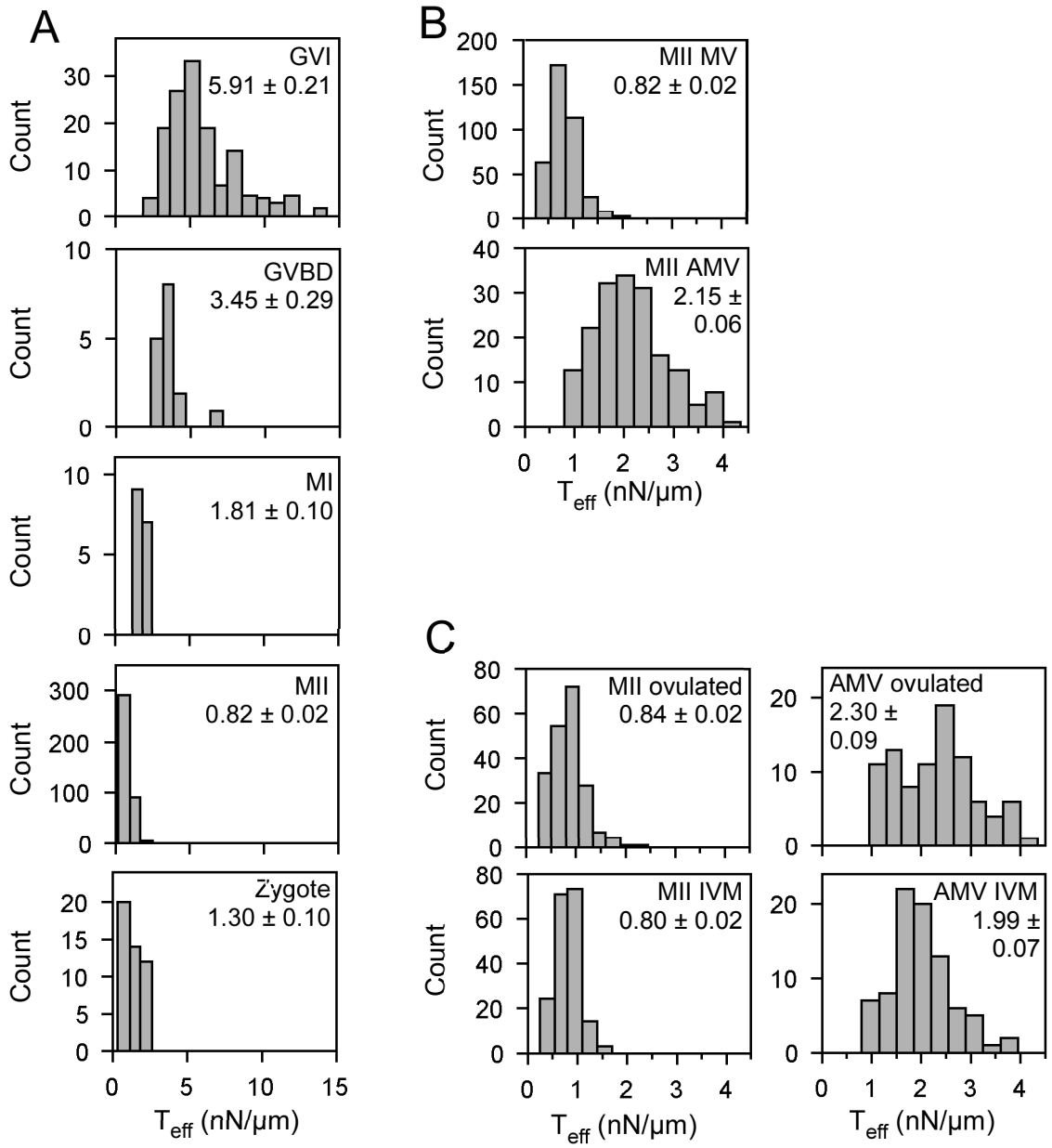
A
GVI
5.91 ± 0.21
GVBD
3.45 ± 0.29
MI
1.81 ± 0.10
MII
0.82 ± 0.02
Zygote
1.30 ± 0.10
Count
T_eff (nN/µm)
B
MII MV
0.82 ± 0.02
MII AMV
2.15 ± 0.06
C
MII ovulated
0.84 ± 0.02
AMV ovulated
2.30 ± 0.09
MII IVM
0.80 ± 0.02
AMV IVM
1.99 ± 0.07

Figure S1

Supplemental Figure 2

Frequency distributions of effective tension measurements in experimentally manipulated oocytes and eggs

These histograms correspond to the data presented in Figures 2B, 3M, and 5B. Each graph is a frequency distribution, with the x-axis indicating T_{eff} (in nN/μm) and the y-axis indicating the number of cells with the indicated T_{eff}. Values shown for each group are the mean ± SEM. Each set of graphs for a given panel has the same scale on the x-axes. Panel A shows the comparison of cytochalasin D (Cyto D)-treated GVI oocytes (n = 75) to solvent-exposed control oocytes (DMSO, n= 43). Panel B shows ML-7-treated GVI oocytes (n = 53) to solvent-exposed control oocytes (DMSO, n= 45). Panel C shows four graphs with comparisons of T_{eff} on the microvillar (MV) domain of ML-7-treated MII eggs (n = 84) and solvent-exposed control eggs (DMSO, n= 79), and T_{eff} on the amicrovillar (AMV) domain of ML-7-treated eggs (n = 36) and solvent-exposed controls (n = 23). Panel D shows control MII eggs (All MII, n = 387), all eggs injected with DN-RDX cRNA (All DN-RDX, n = 65), eggs that were confirmed to be expressing DN-RDX protein and have reduced pERM (DN-RDX exp, n = 8), batch-matched uninjected control eggs (n = 10) and water injected eggs (n = 7).

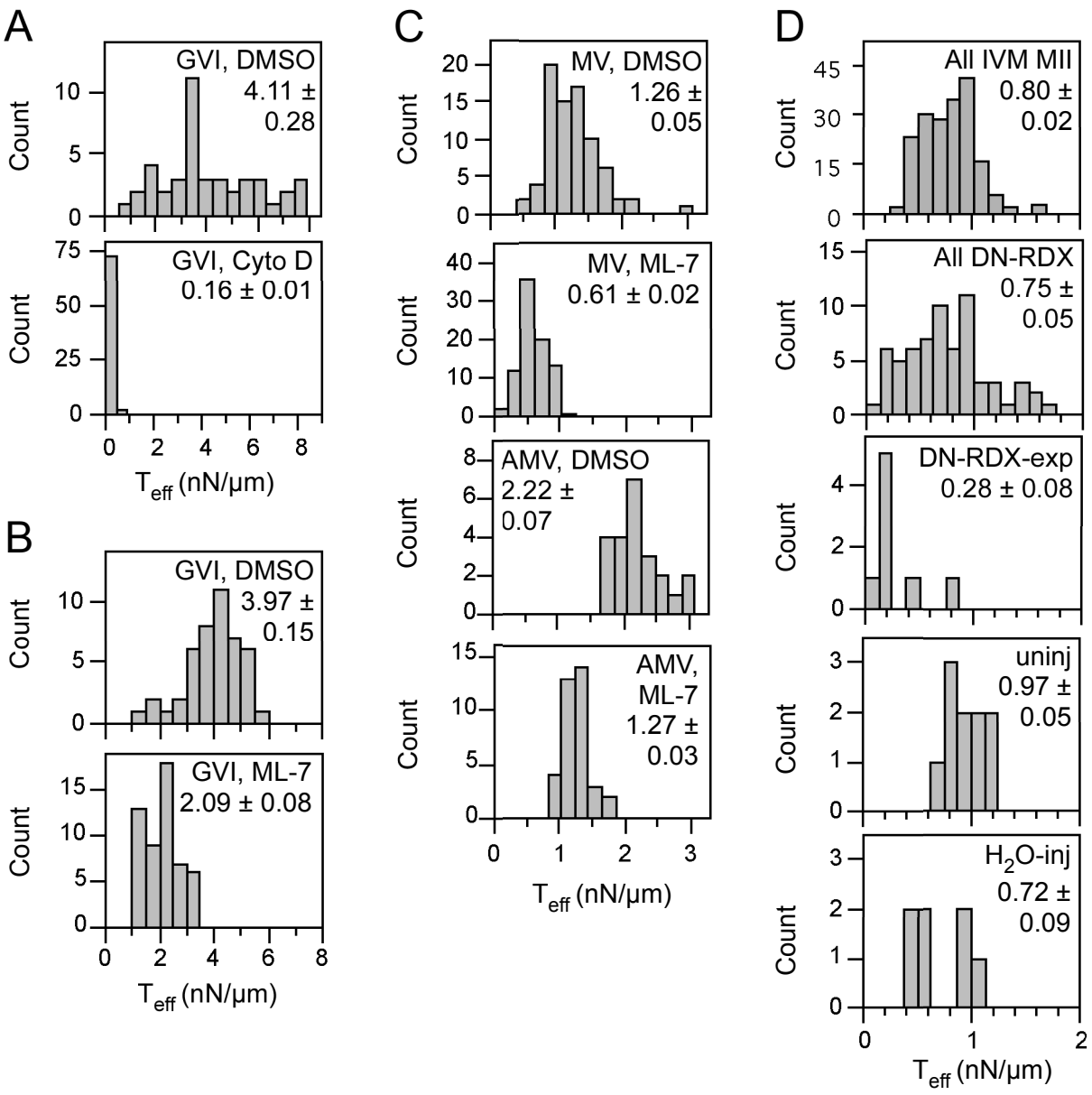
A
GVI, DMSO
4.11 ±
0.28
GVI, Cyto D
0.16 ± 0.01
Count
T_{eff} (nN/μm)
B
GVI, DMSO
3.97 ±
0.15
GVI, ML-7
2.09 ± 0.08
C
MV, DMSO
1.26 ±
0.05
MV, ML-7
0.61 ± 0.02
AMV, DMSO
2.22 ±
0.07
AMV,
ML-7
1.27 ±
0.03
D
All IVM MII
0.80 ±
0.02
All DN-RDX
0.75 ±
0.05
DN-RDX-exp
0.28 ± 0.08
uninj
0.97 ±
0.05
H_2O-inj
0.72 ±
0.09

Figure S2

Supplemental Figure 3

Effects of ConA on effective tension and related phenomena in eggs

Panel A shows the frequency distributions of effective tension measurements in ConA-treated eggs (microvillar domains, n = 89; amicrovillar domains, n = 52) and in untreated metaphase II eggs cultured in parallel (microvillar domains, n = 61; amicrovillar domains, n = 35). These histograms correspond to the data presented in Figure 3L. The difference between microvillar T_{eff} in ConA-treated and untreated eggs is statistically significant ($p < 0.001$); the difference between amicrovillar T_{eff} in ConA-treated and untreated eggs is not statistically significant ($p = 0.14$; Mann-Whitney U test). Panels B and C shows immunofluorescence analysis of the localization of pERM (B) and pMRLC (C) in ConA-treated eggs (ii, iii) and untreated controls (i). The localizations of both pERM and pMRLC were not dramatically different between controls and ConA-treated eggs. ConA treatment did, however, affect cell morphology in some (but not all) eggs; a subset of ConA-treated eggs had a distended amicrovillar domain, and these eggs had somewhat less organized pMRLC staining (illustrated in Panel Ciii). Panel D shows the experimental design and results of assessment of the effects of ConA treatment on second polar body emission. We found that *in vitro* fertilization (IVF) works very poorly in the presence of ConA, as the presence of ConA causes sperm agglutination. IVF also did not work with eggs pre-treated with ConA; the lectin most likely blocks key receptors on the egg surface. Therefore, we inseminated eggs for 30 min in the absence of ConA (to allow the sperm to fuse with the eggs), and then transferred the eggs to medium containing 100 µg/ml ConA and cultured the eggs for 90 min. This resulted in 56/58 control eggs emitting the second polar body, and 41/41 of ConA-treated eggs emitting the second polar body (data from three separate experiments). It is important to note that this lack of an effect on polar body emission could be

due to having to introduce ConA treatment after zygote creation, and that this exposure to ConA was not sufficient to induce abnormalities in polar body emission. An alternative (and not mutually exclusive) explanation is that the change in tension induced by ConA is not sufficient to induce significant abnormalities during polar body emission.

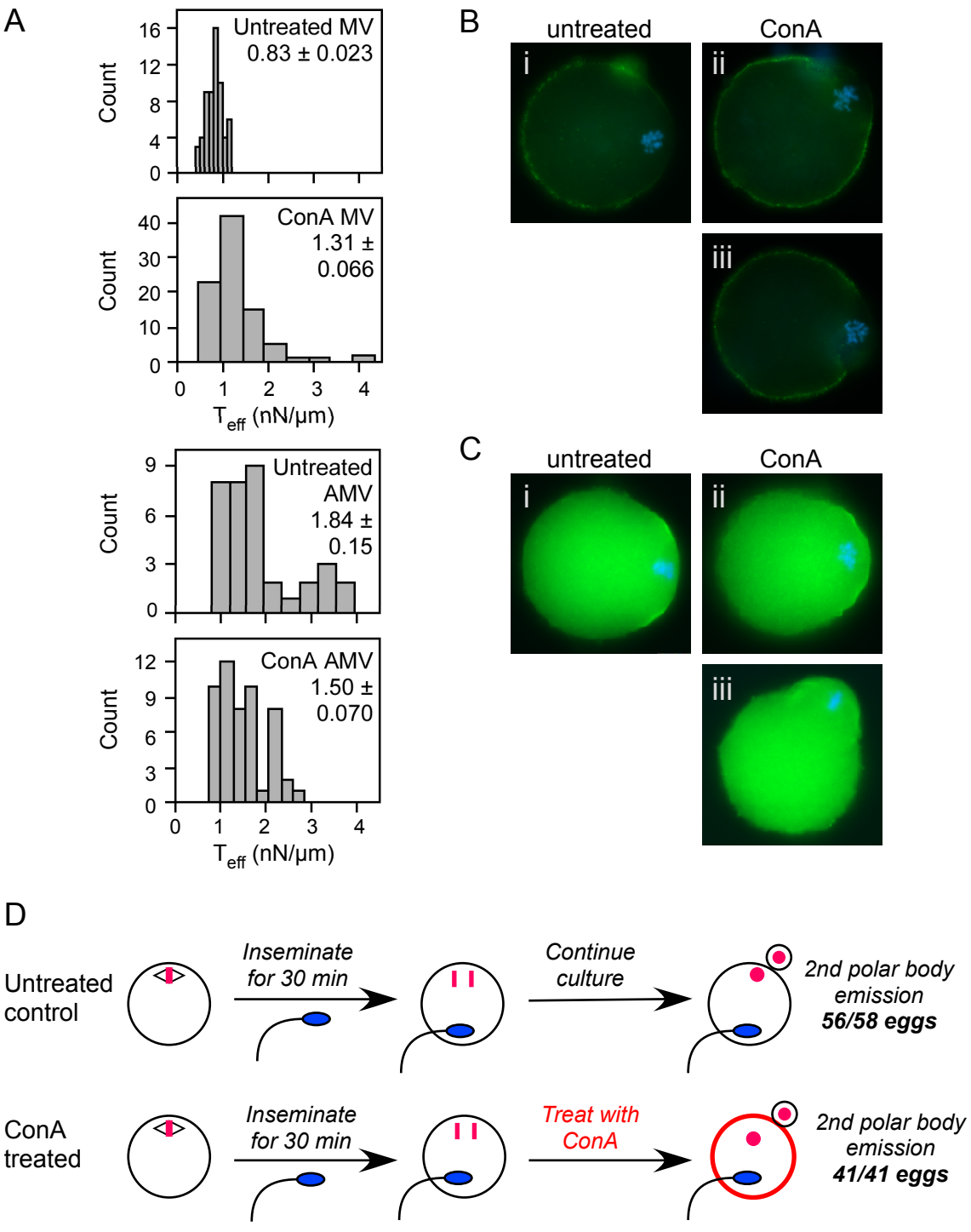
A
Untreated MV
0.83 ± 0.023
ConA MV
1.31 ±
0.066
Untreated
AMV
1.84 ±
0.15
ConA AMV
1.50 ±
0.070
Count
T_eff (nN/μm)
B
untreated
ConA
i
ii
iii
C
untreated
ConA
i
ii
iii
D
Untreated
control
Inseminate
for 30 min
Continue
culture
2nd polar body
emission
56/58 eggs
ConA
treated
Inseminate
for 30 min
Treat with
ConA
2nd polar body
emission
41/41 eggs